Forschung im Ingenieurwesen (2025)89:112
https://doi.org/10.1007/s10010-025-00887-y

ORIGINALARBEITEN/ORIGINALS

Experimental study on the condition monitoring of planetary journal bearings in wind turbine gearboxes using the surface acoustic wave method

Thomas Decker[1] · Georg Jacobs[1] · Julian Röder[1] · Tim Scholz[1] · Christoph Paridon[1] · Tim Schröder[2]

Received: 10 June 2025 / Accepted: 1 August 2025

Abstract

Hydrodynamic journal bearings are a driver of increasing power density and reliability of wind turbine gearboxes. Despite their high fatigue reliability operating in hydrodynamic conditions, journal bearings can be damaged quickly in the event of a critical operating condition with solid body contact (e.g. severe overload and mixed friction or failure of the lubricant supply). In the worst-case scenario, bearing damage occurs suddenly with no clear warning period. To reduce the risk of damage condition monitoring systems (CMS) can be installed for the continuous monitoring of the bearing's operating condition. In the event of a critical condition countermeasures can be taken immediately (e.g. derating the wind turbine) to reduce the damage risk. This approach has the potential to further increase wind turbine reliability and reduce costs resulting from downtime and maintenance. However, commercial CMS for journal bearings in wind turbines with the required level of readiness for field operation have not yet been fully developed and thoroughly tested. One monitoring technique potentially capable of detecting the change from normal to critical operating conditions immediately is based on surface acoustic waves (SAW). This work presents the results of an experimental study of planetary journal bearings equipped with a CMS based on the SAW method. The aim of this work is the proof of concept of the condition monitoring method based on SAW in a planetary journal bearing and the demonstration of the transferability of the SAW method from small radial journal bearings to planetary journal bearings. The results show that different friction states can be detected using the SAW method. The paper gives insights to the application of the measuring equipment, the operation conditions analyzed and into the analysis of the data. The CMS for the planetary journal bearing based on SAW presented here is the first of its kind and represents a major step towards the continuous monitoring of journal bearings in wind turbine drive trains. Through a future introduction of a fully developed SAW-based CMS in the field application in wind turbines an early detection of critical operating conditions for journal bearings can be achieved. Thus, the prevention of gearbox damage and the reduction of costs for operation and maintenance due to journal bearing failures can potentially be made possible.

1 Introduction

Wind energy makes the largest contribution to the electricity supply from renewable energy sources. Wind energy covered over 27% of Germany's electricity consumption in 2023, making it the most important energy source in the German electricity mix ahead of fossil fuels [1]. To further improve wind energy competitiveness, technological research and development are focusing on the reduction of the levelized costs of electricity (LCOE). Increasing the reliability of wind turbines (WT) plays a decisive role here, as costs for maintenance and repair of damage to WTs can account for up to 30% of the LCOE [2]. One technological advancement contributing to a increased reliability of drive trains in WTs in recent years is the use

This article is based on a previous contribution of some of the authors to "VDI Fachtagung Gleit- und Wälzlager 2025".

✉ Thomas Decker
thomas.decker@cwd.rwth-aachen.de

[1] Chair for Wind Power Drives, RWTH Aachen University, Campus-Boulevard 61, 52074 Aachen, Germany

[2] Vestas Nacelles Deutschland GmbH, Martin-Schmeißer-Weg 18, 44227 Dortmund, Germany

Published online: 26 August 2025

of hydrodynamic journal bearings as planetary gear bearings in the gearboxes [3]. Journal bearings can be operated without wear if designed correctly. Their compact design allows gearboxes to be designed with a higher torque density compared to rolling bearings [4]. For these reasons, journal bearings have already been used successfully in the field as planetary gear bearings for WTs for a number of years [5]. Despite their high reliability and robustness, there are events that pose a risk of damage to journal bearings WT gearboxes such as strong mixed friction (e.g. due to overload), overheating, failure of the lubricant supply [6], or contamination of the lubricant with particles [7]. These conditions can eventually lead to wear on the bearing and, in the worst case, to a sudden component failure. Condition monitoring systems (CMS) can be used to prevent damage to machine components and reduce downtimes. These systems record information about the operating and degradation state of a machine component and communicate with the system controller in the event of a critical condition to prevent component failure. Technically established solutions already exist for monitoring rolling bearings and gears in WT drive trains [8]. Condition monitoring of tooth flanks or rolling bearings mainly focuses on crack propagation, degradation, or fatigue progress of the component and on deriving a remaining useful lifetime (RUL) to schedule repair efficiently. Conversely, journal bearings are not susceptible to fatigue. In addition, journal bearing damage is often caused by the above-mentioned operating anomalies and adhesive wear rather than the relatively slow progression of abrasion. Therefore, instead of a RUL prediction, condition monitoring of journal bearings often focuses on determining the current load condition (load monitoring) to detect and prevent critical mixed friction events with a low latency. This concept of measuring the current operating condition of journal bearings in WT gearboxes is currently still the subject of research and development and is referred to below as condition monitoring.

A few approaches for the condition monitoring of journal bearings are discussed in the relevant literature: Apart from the measurement of acoustic emission [9, 10] or temperature [11, 12], the measurement of surface acoustic waves (SAW) is a CMS metric with high potential [13, 14]. The SAW approach is known for its good sensitivity to friction conditions in tribological systems (e.g. roller bearings [13]). The SAW method has already proven to be suitable for detecting friction conditions (e.g. mixed friction) in hydrodynamic radial journal bearings. It has also been demonstrated before that measuring SAWs in a journal bearing during operation can enable the prediction of the oil film height by means of machine learning [15]. In addition, the sensitivity of the propagation behavior of SAWs in a journal bearing to a lubricant shortage or contamination of the lubricant with particles was shown. These anomalous events can be detected via the change in the SAW signal pattern [16]. The existing work on the application of the SAW method to journal bearings is limited to experimental investigations at an abstract level (small bearings on a component test rig). Further investigations are needed for the application of the SAW method on planetary journal bearings in WT gearboxes. The aim of this work is to demonstrate the transferability of the SAW method from radial journal bearings with a small B/D ratio as presented in [15] to planetary journal bearings. For this purpose, experiments are carried out on two different journal bearing test rigs equipped with SAW sensors and the measurement results are compared. The test results are compared in terms of load and speed sensitivity and prediction of the friction state is carried out. The prediction is done using a machine learning (ML) classification algorithm. The prediction quality of both a multi-layer perceptron (MLP) and a long short-term memory (LSTM) neural network are compared.

2 Method

The basics of the SAW method are explained in detail in [17] and the application to journal bearings is demonstrated in [15]. SAWs are actively excited ultrasonic waves that propagate along the surface of a solid substrate, the so-called wave guide. In the context of this work, the sliding surface of the journal bearing acts as the wave guide. Figure 1 shows the SAW sensor setup for a radial journal bearing. The system comprises two piezo-electric probes: emitter and receiver.

The probes are glued into inward-facing radially boreholes underneath the sliding surface. The load zone (area of

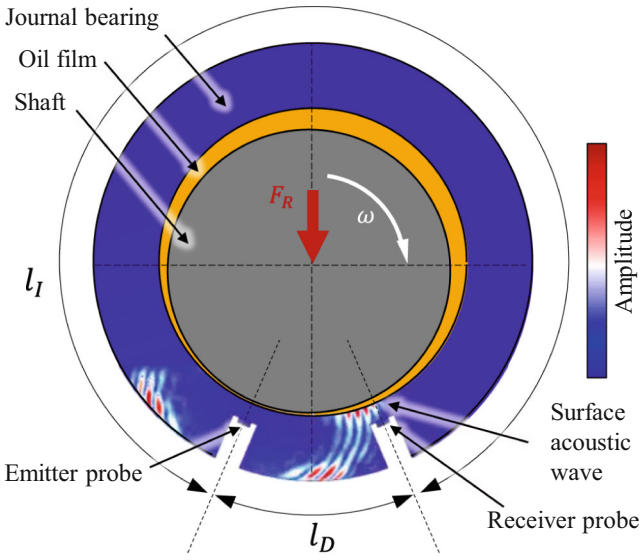

Fig. 1 Schematic visualization of the SAW setup on a radial journal bearing [15]

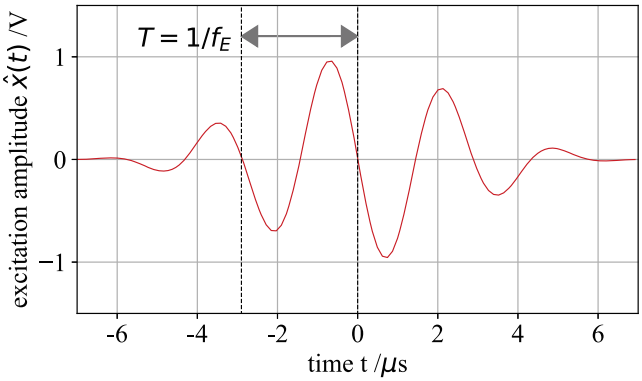

Fig. 2 SAW excitation signal $\hat{x}(t)$

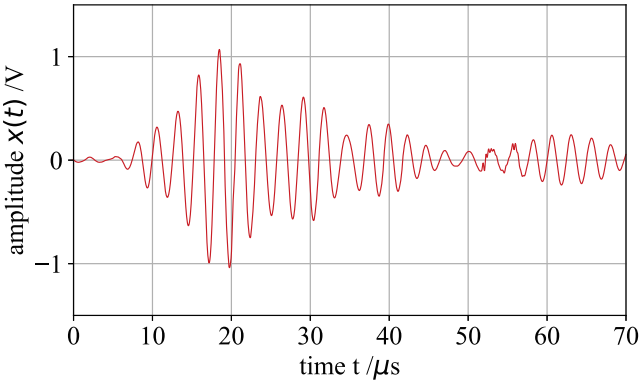

Fig. 3 Received SAW signal $x(t)$

smallest oil film height h_{min}, and highest total pressure p_t) is located between the two probes. This arrangement of the probes ensures that the SAWs propagate directly through the load zone. The smallest distance on the sliding surface between the two probes is referred to as the direct acoustic path length l_D. The SAW measurement is a cyclic process executed multiple times per second [14]. During one excitation cycle with duration t_C the excitation signal $\hat{x}(t)$ is emitted by the emitter probe and the response signal x(t) is measured by the receiver probe. In Fig. 2 an exemplary excitation wavelet is shown for f_E = 350 kHz.

In this work, the excitation signal is a transient burst containing a sinusoidal wavelet with the excitation frequency f_E that is equivalent to [15]. The response signal x(t) measured by the receiver probe is shown in Fig. 3.

The change in the propagation behavior of x(t) between two excitation cycles provides information about the operating status of the bearing and can be evaluated using various measured variables:

The propagation time τ and amplitude A are measured at one particular phase of x(t) specified by the gate position parameter t_G. The integral value σ describes the amplitude integral of $x(t)$ within a certain range defined by the parameters t_0 and Δt.

$$\sigma = \int_{t_0}^{t_0+\Delta t} x\,(t)\,dt \tag{1}$$

The evaluation parameters t_G, t_0, and Δt must be defined specific to the receiver signal and are often chosen in the range of the first wave packet that arrives at the receiver (e.g. 10μs in Fig. 3). This ensures that the evaluation refers to a wave packet that has traveled the shortest path l_D through the load zone. This is crucial, as an inversely running wave packet (path l_I in Fig. 1) does not interact with the load zone of the bearing, and is therefore unsuitable for evaluating the friction condition.

2.1 Transfer of the SAW method to planetary journal bearings

The propagation characteristics and thus also the quality of the measurement performed by a CMS based on SAW depend not only on the parameterization of the measurement (excitation parameters, gate position t_G and integral range t_0 + Δt) but also on substrate material, the coating (e.g. lubricant), bearing clearance, and the length of the path l_D. For this reason, the transferability of the SAW method from small radial journal bearings to planetary journal bearings must be explicitly investigated and evaluated. Tests on both radial journal bearings (RJB) and planetary journal bearings (PJB) equipped with the SAW measurement technology are conducted and compared as part of this work. For the RJB test the same setup as described in [15] is used. Both bearing types are manufactured with the same material (CuSn12Ni2-C) and the lubricant used in the experiments is identical (ISO VG 320—PAO). A detailed comparison of the bearing parameters of the two types of test bearings used for this work is given in Table 1.

In Fig. 4, the measurement setup for the RJB is shown. Both SAW probes are located at the same axial position (at

Table 1 Bearing parameters describing the two test scenarios (RJB and PJB) used in this work

Parameter	Symbol/unit	Test rig	
		RJB	PJB
Bearing width	B/mm	30	115
Bearing diameter	D/mm	120	100
B/D-ratio	B/D/–	0.25	1.2
Rel. clearance	$\psi/permil$	1.1	1.1
Profile crowning	R/μm	0	50
Acoustic path ratio	α/–	0.14	0.72
Direct path length	l_D/mm	47	153

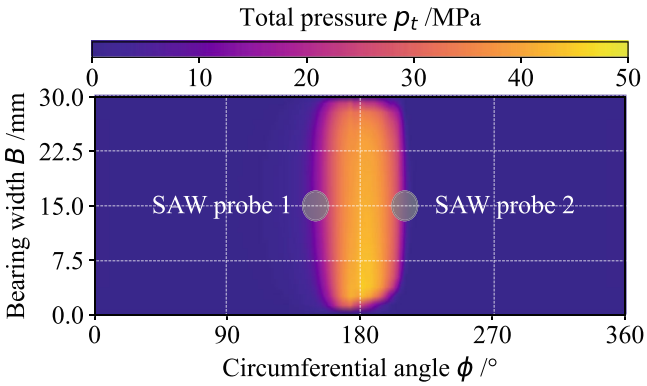

Fig. 4 SAW sensor setup on the radial journal bearing (RJB) component test rig relative to the pressure distribution

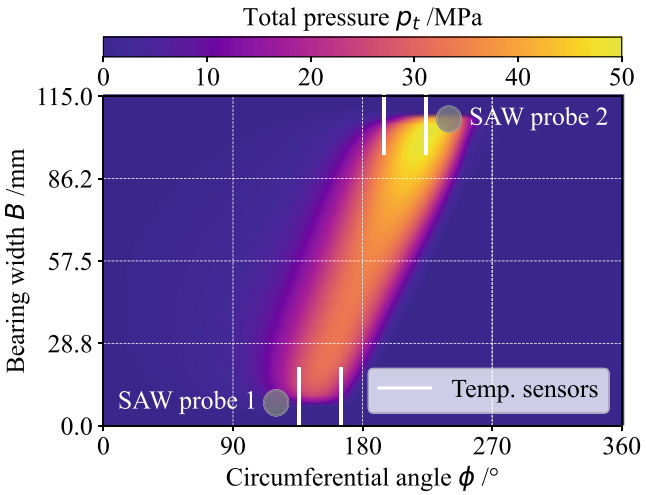

Fig. 5 SAW sensor setup on the planetary journal bearing test rig (PJB) relative to the pressure distribution

B = 15 mm) with the load zone indicated by the plot of the pressure distribution located between both SAW probes.

Unlike the RJB on the component test rig, the PJB does not experience uniaxial load (or radial load). It is also subjected to a skew moment caused by the axial tooth forces in addition to the radial force. This skew moment and the tilted load zone (indicated by the pressure distribution in Fig. 5) is typical for journal bearings of helical planetary gears, such as those used in WT gearboxess. To cover the entire load zone of the planetary journal bearing (area of high hydrodynamic pressure) with the SAW method, the emitter and receiver probes are positioned axially offset ($B_{probe\,1} = 5\,mm$, $B_{probe2} = 100\,mm$), unlike in the RJB application. This design of the SAW setup leads to a larger acoustic path length l_D between the SAW probes on the PJB compared to the RJB (see also Table 1). The ratio α of the direct acoustic path length to the inverse path (Eq. 2) is also greater on the PJB than on the RJB which hampers the distinction between the SAW signal portions that propagate directly through the load zone and the portion that propagate inversely. It must be verified whether this arrangement allows for a sufficiently precise measurement on the PJB.

$$\alpha = \frac{l_D}{l_I} \tag{2}$$

The measurement setup for the planetary bearing is shown in Fig. 5.

The PJB is a thin bronze sleeve that is mounted on the planetary axle with a cylindrical press fit. Similar to the RJB, the SAW probes are glued into boreholes underneath the sliding surface. For this purpose, boreholes are drilled in the planet axle through which the SAW probes are inserted into the pin material. A photograph of the PJB on the axle equipped with the SAW probes is shown in Fig. 6a. The assembled planetary bearing test rig is presented in Fig. 6b. The test rig consists of three gears, where the meshing of a real planetary gear between the ring gear and sun gear can be reproduced. The planetary gear (center) is pressed onto the stationary planet pin by the drive and output pinion. This

a

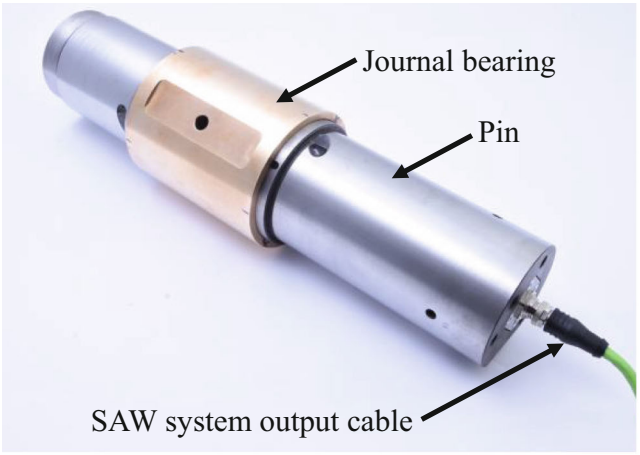

b

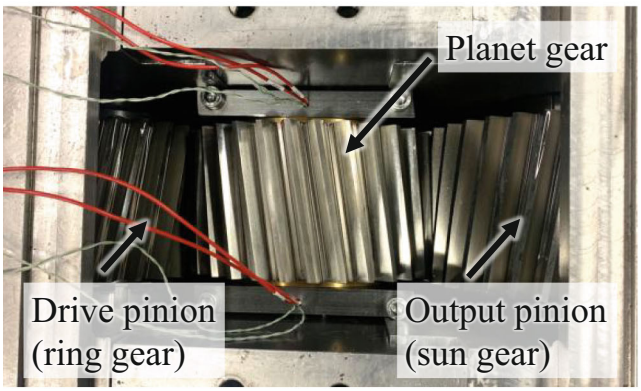

Fig. 6 **a** Photograph of the planetary journal bearing (PJB) on the pin with integrated SAW measurement setup, **b** Photograph of the assembled gear configuration with the PJB on the test rig

results in the load distribution characteristic of planetary journal bearings (see also Fig. 5).

2.2 ML-based determination of the operating condition

For the evaluation of the operating condition of the journal bearings, a metric indicating the friction state is used in this work. The Λ ratio (see Eq. 3) is often used as an indicator of the operating condition of a journal bearing (distinction between hydrodynamic operation and mixed friction). It describes the relation between the minimal oil film thickness in the bearing h_{min} and roughness values $R_{q,i}$ of the bearing itself and its counterpart:

$$\Lambda = \frac{h_{min}}{\sqrt{R_{q,1}^2 + R_{q,2}^2}} \tag{3}$$

In the literature, Λ = 3 is often specified as the transition point between hydrodynamics and mixed friction [17]. The minimal oil film height h_{min} can be assumed to be a function of the sliding speed v_S and load $\overline{p}$ (temperature, lubricant condition and viscosity influences are neglected in this work for the sake of simplicity):

It is assumed that the sliding speed v_S in the real application (e.g. WT gearbox) is approximately known to the CMS controller in real time via a sufficiently accurate analytical model or easily measurable.

A regression model $\Theta_i\left(\vec{x}_i\right)$ is used to predict the external load $\overline{p}$. The input vector $\vec{x}_i$, at the time step i consists of selected SAW signal features (e.g. signal amplitude A and propagation time τ at the gate position t_G, and the signal integral σ). In addition, the sliding speed v_S is also included in the model input $\vec{x}_i$. On both the RJB and PJB, the cycle time t_D is set to 1 ms. To remove potential noise and high-frequency signal components the raw data is smoothed over a defined time interval t_D using a floating mean value filter to create the model input $\vec{x}_i$.

$$\overline{p}_i = \Theta_i\left(\vec{x}_i\right) \tag{4}$$

The approach according to Eq. 4 has a time-continuous model output $\overline{p}_i$ for each time step i, and therefore differs from the ML model presented in [15], where a direct classification of lambda was performed. It is expected that the existing method from [15] can be improved by the continuous determination of $\overline{p}$, as this allows the model output to be compared directly with the external load. This assumption must be verified on the basis of the test results. For a robust determination of the specific pressure $\overline{p}$ using Eq. 4, the load sensitivity of the SAW measurement should be as high and uniform over the whole range of operating points, as possible.

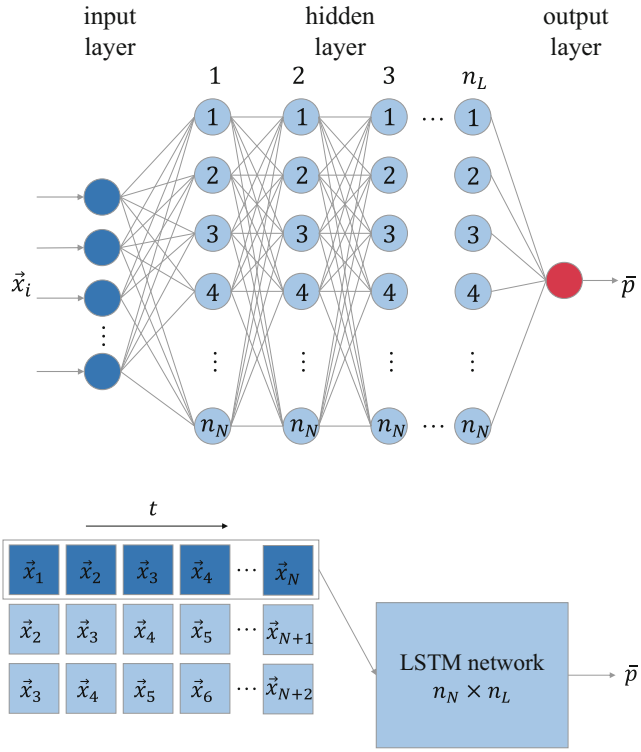

Fig. 7 Schematic depiction of the architecture of a multi-layer perceptron network

For this work, two different machine learning model architectures are considered: the multi-layer perceptron (MLP) and the long short-term memory (LSTM). The MLP's architecture is defined by two hyperparameters: number of hidden layers n_L and number of neurons per hidden layer n_N (see also Fig. 7). In previous work, it has been demonstrated that MLPs can be used for the detection of critical operating conditions in RJBs using SAW measurements with a classification accuracy of around 90% [15].

The MLP takes the vector $\vec{x}_i$ at a specific time i, as input and therefore cannot evaluate the signal behavior over time (e.g. modulation frequency). An alternative approach is represented by so-called recurrent neural networks, such as the LSTM. In this type of model, the connections of a neuron to the next layer are supplemented by a cyclic connection to itself again. In addition to the aforementioned hyperparameters, the time length of the input sequence N is a relevant parameter for the LSTM network. It is assumed that the detection accuracy can be further improved by using the LSTM network compared to the MLP approach. This also needs to be verified.

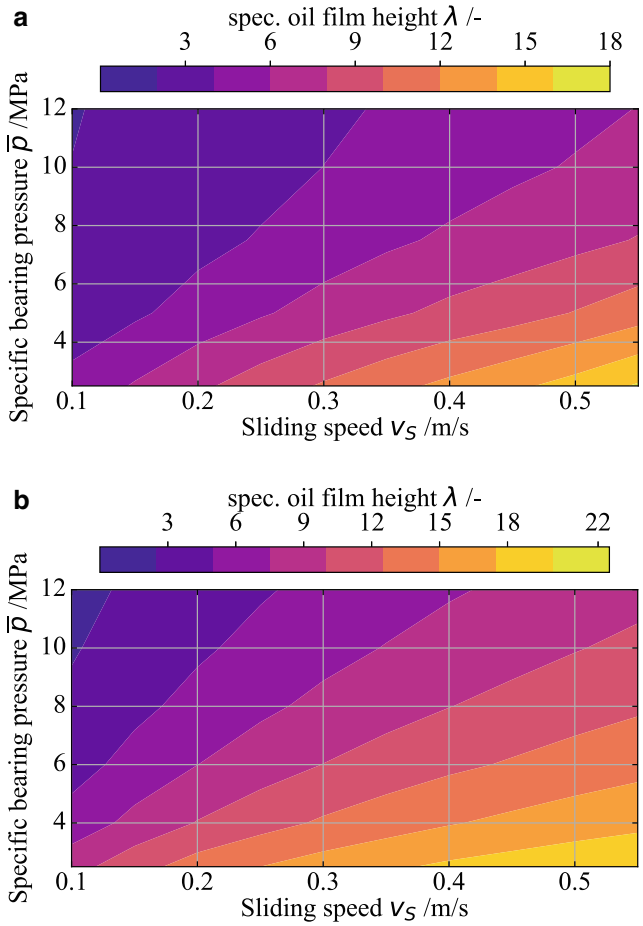

Fig. 8 Distribution plot of the specific oil film height Λ over sliding speed v_S and specific pressure $\overline{p}$ for the RJB (**a**) and the PJB (**b**) simulated with EHD-models

2.3 Definition of the test procedures

In this work, the values for Λ were calculated as a function of $\overline{p}$ and v_S using EHD simulations of the two journal bearings. For the sake of simplicity $\Lambda(\overline{p}, v_S)$ is calculated under the assumption of a constant bearing temperature. In Fig. 8, the specific oil film height Λ is shown for the RJB and PJB. Due to the different bearing geometries (see also Table 1), the distributions of the specific oil film height differ between RJB and PJB. The critical limit of $\Lambda = 3$ on the PJB is reached at significantly greater load compared to the RJB.

Different procedures were defined for both test campaigns as part of this work to encompass a specified operating range. To establish comparability between the two tests, the Sommerfeld number So was used as an equivalence criterion according to Eq. 5.

$$So = \frac{\overline{p} \cdot \psi^2}{\eta \cdot \omega} \tag{5}$$

The specific pressure $\overline{p}$ and the sliding speed v_S were set so that equivalent Sommerfeld numbers were achieved on both test rigs during the experiments.

3 Results

This chapter discusses the SAW measurement results of the experimental campaigns, on the RJB and the PJB test rig. The achieved sensitivity of the SAW data regarding the operating conditions is compared. Subsequently, the generation of two data sets and the training of regression models for predicting the operating point using SAW measurement data are described, and the prediction results of the models are discussed.

Numerous experiments were carried out for both bearing types (RJB and PJB), and the measurement data for training the MLP regression was combined into one data set each. Each data set contains measurements from start-stop tests and test runs in which the entire operating range of the journal bearing is covered. In Fig. 9, an excerpt of the start-stop experiment from the PJB test is shown. Sliding speed v_S and specific bearing pressure $\overline{p}$ are shown in the upper plot. One start-stop cycle lasts around 40 sec and the operating point ($\overline{p}$ and v_S) reached within each cycle is varied with each cycle to achieve a certain variance in the training data and thus robustness in the regression. The SAW propagation time measurement τ is shown in the lower plot. It was demonstrated before, that for the RJB application the characteristic SAW features (such as the propagation time τ) modulate with the rotational frequency ω of the shaft [15]. This observation can also be made for the PJB as the propagation time signal modulates during the start-stop cy-

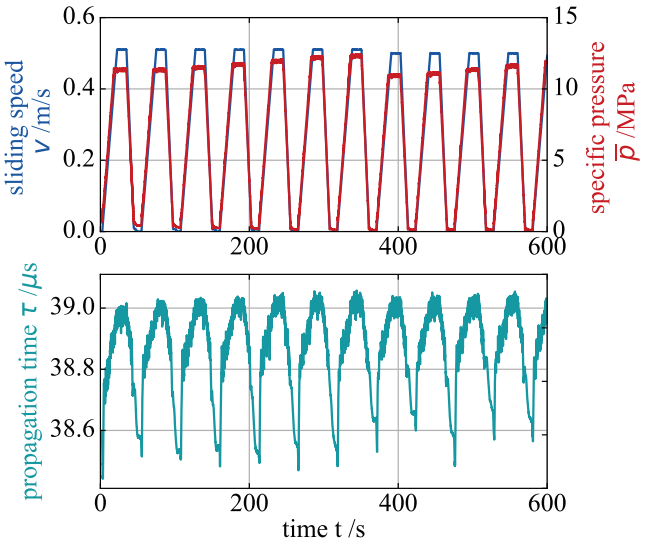

Fig. 9 SAW propagation time measurement from the start-stop experiment on the PJB test rig

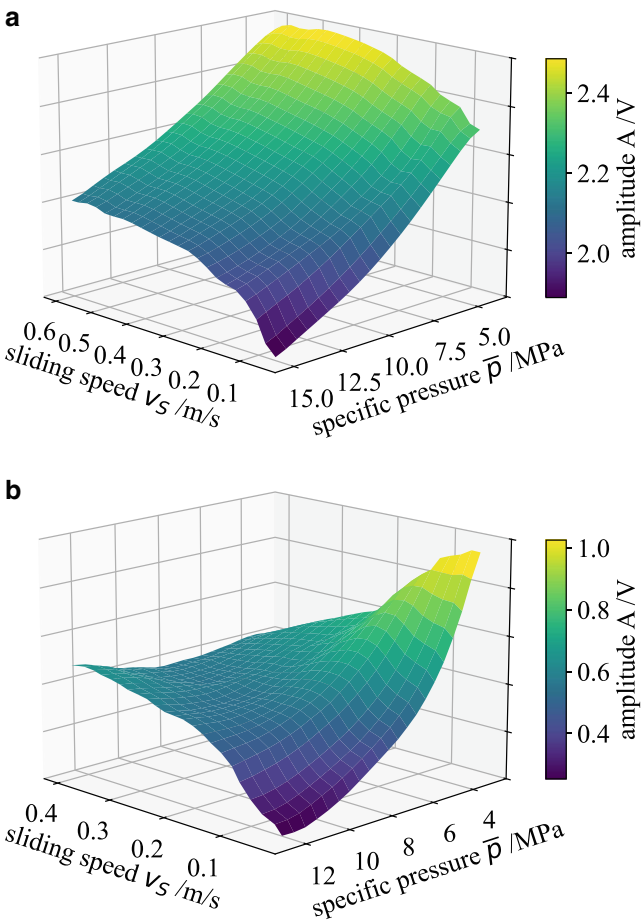

Fig. 10 Measurement results for the SAW integral value relative to the sliding speed and specific pressure for the RJB test rig (**a**) and the PJB test rig (**b**)

cle (see Fig. 9). The modulation increases with the speed of the planet gear (sliding speed v_S).

3.1 Load and speed sensitivity

In previous work, it has been shown that SAW signal features (e.g. the integral value σ) are sensitive to the minimal oil film height h_{min} in a journal bearing [15]. In Fig. 10, the SAW measurement results for the RJB (a) and PJB (b) are shown in comparison. The surface plots show the SAW amplitude value A as a function of specific pressure $\overline{p}$ and sliding speed v_S. It is noteworthy that the SAW amplitude is significantly more sensitive to the specific pressure on the RJB than on the PJB. Particularly at a high sliding speed (approx. $0.4\,m/s$), only a small variance (gradient) of the SAW amplitude on the PJB can be observed with varying pressure. One possible explanation for this may be the increased acoustic path length l_D on the PJB (c.f. Table 1). At small sliding speed (approx. $0.1\,m/s$), a good sensitivity to the specific pressure is achieved at the PJB as well.

Table 2 shows the largest and smallest values for the load and speed sensitivity derived from the measurement of the SAW amplitude value A in Fig. 10. For a robust determination of the specific pressure $\overline{p}$ using Eq. 4, a load sensitivity that is as uniform and high as possible is desirable. The results show that the load and speed sensitivity depend on the operating point. The integral values σ for the RJB and the PJB show the same behavior.

In addition, it must be investigated whether the apparently lower load sensitivity has a negative influence on the prediction accuracy of the machine learning models.

3.2 Surrogate model validation

To train the surrogate models (MLP and LSTM), a training dataset is used that contains data comprising the entire $\overline{p}$–v_S envelope shown in Fig. 10, as well as start-stop experiments as shown in Fig. 9. In total, the training dataset covers an experiment duration of 13 h. The quality criterion of the regression *MSE* (mean square error) is used to compare the load prediction of the surrogate model $\Theta_i\left(\vec{x}_i\right)$ with the actual load applied $\overline{p}_i$ (see Eq. 6).

$$MSE = \frac{1}{m}\sum_{i=1}^{m}\left(\Theta_i\left(\vec{x}_i\right) - \overline{p}_i\right)^2 \tag{6}$$

In Table 3, the results of the hyperparameter optimization are shown together with the achieved scores of the models on the training data.

The result of the hyperparameter optimization for the LSTM models on RJB and PJB are listed in Table 4.

For the validation of the trained regression models, additional procedures are tested on both test rigs with which the real operation of a WT journal bearing is simulated. The

Table 2 Summary of the measured maximum and minimum speed and load sensitivity of the integral value σ on the RJB and PJB test rig derived from the measurement data shown in Fig. 10

Value	Symbol/unit	Test rig	
		RJB	PJB
Max. speed sensitivity	$\frac{dA}{dv_S}\Big\vert_{max}\,/Vs/m$	1.8825	3.1358
Max. load sensitivity	$\frac{dA}{d\overline{p}}\Big\vert_{max}\,/V/MPa$	−0.0659	−0.2289
Min. speed sensitivity	$\frac{dA}{dv_S}\Big\vert_{min}\,/Vs/m$	0.0008	−0.0004
Min. load sensitivity	$\frac{dA}{d\overline{p}}\Big\vert_{min}\,/V/MPa$	−0.0101	−0.0001

Table 3 Hyperparameters and surrogate model quality results for the optimal MLP networks for regression on the data from RJB and PJB

Value	Symbol/Unit	Test rig	
		RJB	PJB
Hyperparameter			
Number of layers	$n_L/-$	15	8
Number of neurons per layer	$n_N/-$	154	210
Down sampling	t_D/ms	1076	1402
Model quality on the training data			
Mean square error	MSE/MPa	0.171	0.359
Model quality on the validation data			
Mean square error	MSE/MPa	0.024	0.43

Table 4 Hyperparameters and surrogate model quality results for the optimal LSTM networks for regression on the data from RJB and PJB

Value	Symbol/Unit	Test rig	
		RJB	PJB
Hyperparameter			
Number of layers	$n_L/-$	7	4
Number of neurons per layer	$n_N/-$	172	375
Down sampling	t_D/ms	70	364
Sequence length	$N/-$	102	108
Model quality on the training data			
Mean square error	MSE/MPa	0.02	0.118
Model quality on the validation data			
Mean square error	MSE/MPa	0.017	0.293

procedures contain numerous relevant design load cases (DLCs) for journal bearings in WT gearboxes. These DLCs can be described as combinations of load and speed. The IEC 61400-4 design standard for WTs distinguishes different operating conditions for a WT gearbox journal bearing [18]. In Fig. 11, an approximate load-speed envelope curve is shown, on which the validation tests for this work are based.

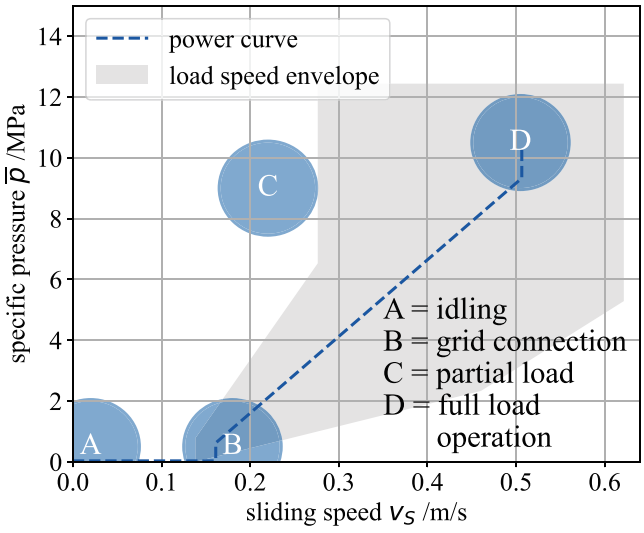

Fig. 11 Operating condition of the journal bearing covered by the test campaign (based on a WT torque speed envelope) (Operating regimes based on [18, , 19])

A comparison between the time series of the real load $\overline{p}$ applied and measured on the test rig (blue curve) and the prediction from the MLP surrogate model (green dotted curve) is given below. In Fig. 12, a section of the validation procedure on the RJB test rig is shown. The validation procedures contain combinations of the load cases A to D shown in Fig. 11. The validation results show that dynamic load changes are well represented by the load regression. There is no significant latency between the actual applied load and the prediction from the surrogate model based on the SAW measurement. However, certain deviations between the actual load and the surrogate model can be observed for the longer load levels indicated by the error values E_{MLP} and E_{LSTM} plotted in red. The maximum deviation is limited to below 2 MPa and no significant difference between the two models can be observed.

Figure 13 shows that the regression result for the PJB is significantly noisier than for the RJB. This is due to a generally noisier input data from SAW measurements to the models. Thus, the MLP, taking a single time sample $\vec{x}_i$ as input, yields a prediction with a comparable quantity of noise. In contrast, the LSTM works with time series as input values and therefore provides predictions that are less noisy over time. The dynamic behavior of the surrogate models is similar for the PJB and the RJB. The validation results from the PJB test show that the maximum deviation of the actual load and the predicted load is greater in steady-state operation than in the RJB test (above 2 MPa). This

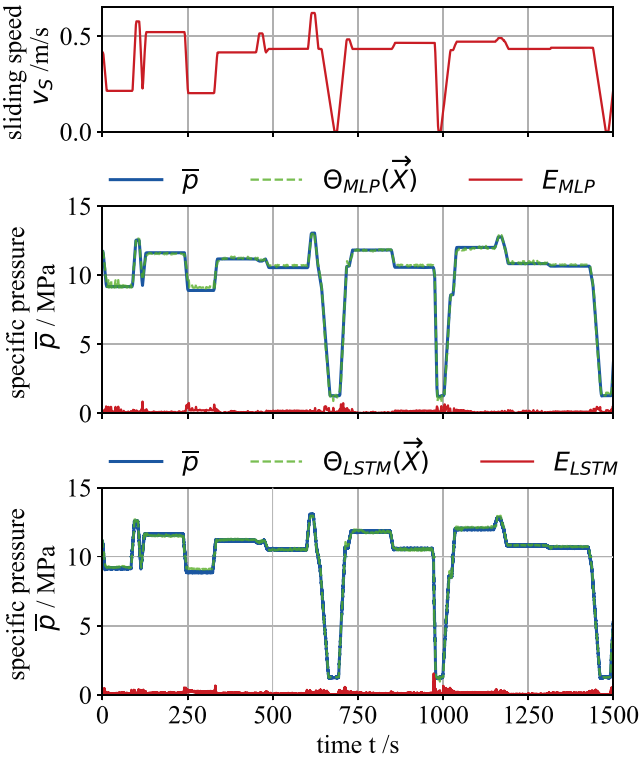

Fig. 12 Load prediction result for the RJB test from MLP and LSTM model

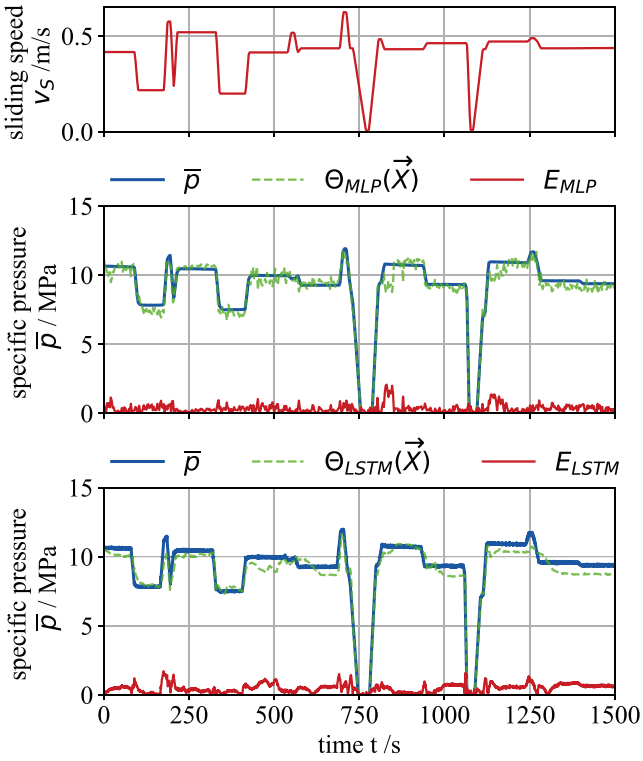

Fig. 13 Load prediction result for the PJB test from MLP and LSTM model

can be explained by the lower load sensitivity on the PJB mentioned above (compare Fig. 10b).

From the results in Figs. 12 and 13, it can be concluded that a good load prediction result can be achieved by extending the training data sets compared to the approach presented in [15], and selecting suitable model parameters for both bearings. The comparison of the machine learning models MLP and LSTM shows that although the LSTM produces less noisy results due to the time-based processing of the data, it has a higher absolute error for the PJB than the MLP. In the following, the MLP is therefore used for the evaluation of the friction state.

Following the load regression using the surrogate models, the friction state Λ is determined on the basis of the SAW measurement data, the predicted bearing load $\Theta_{MLP}\left(\vec{x}_i\right)$. and the EHD results from Fig. 8. In Fig. 14, the results from the friction state calculation on RJB and PJB are shown in comparison. The friction state prediction Λ (green dotted curve) is interpolated from the EHD results as a function of the sliding speed v_S and the prediction result for the load $\Theta_{MLP}\left(\vec{x}_i\right)$.

The threshold value for the transition from hydrodynamic operation to mixed friction ($\Lambda = 3$) is indicated with the horizontal grey line. A specific oil film height (friction state) Λ less than 3 mainly occurs during start and stop processes (e.g. t = 700 sec and t = 1000 sec in Fig. 14). During the presented time frame, both bearings do not experience the exact same values for Λ. This can be explained by using the Sommerfeld number *So* as the criterion for transferring the test procedures from the RJB test rig to the PJB. This approach merely approximates the operating states of the bearings. Nonetheless, a precise prediction of the specific oil film height is achieved on both bearing types.

4 Discussion and outlook

This paper discusses an approach to determine the frictional state of a planetary journal bearing using SAW measurements. The existing method for a radial journal bearing was successfully transferred to a planetary journal bearing. The SAW measurement data was used to train machine learning models (MLP and LSTM) for a prediction of the friction state Λ based on regression. The results show that the MLP model yields the best prediction of the friction state for both test applications demonstrated in this work.

The present study has demonstrated the capability of a SAW-based CMS in predicting the lubricant film height and therefore the operating condition of a journal bearing. In an online application this status information about the operating condition can be transferred to a WT controller, aiding in the avoidance of critical states. However, before this method can be integrated into a real turbine controller software and tested in the field, further validation is required,

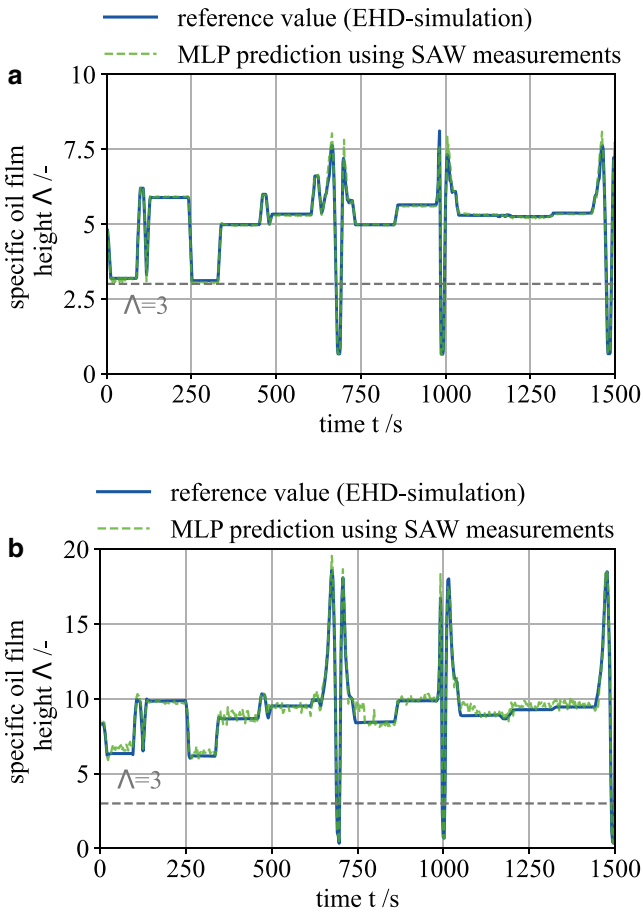

Fig. 14 Time series for the prediction of the specific oil film height Λ for the RJB MLP (**a**) and for the PJB MLP (**b**)

which will be conducted in a full-size WT gearbox test. Thus, future studies will address the behavior of a SAW-based CMS for planetary journal bearings in a real wind turbine gearbox to further increase the confidence in the method. This is necessary since the experiments presented in this work are limited to component test rigs.

In the context of this work, the parameterization of the SAW measurement (excitation frequency, number of cycles of the excitation wavelet, position of the gates, etc.) is done manually. This involves a high degree of uncertainty for parameterization errors. Depending on the choice of parameters, the measurement of the SAW characteristic values may only have a low load or speed sensitivity. To further improve the method shown here, it is advisable to develop an optimization approach for the SAW parameterization, for example. Such a method will be addressed in future work.

As part of this work, the design decision for the SAW application on the PJB (positioning of the SAW probes) was made on the basis of empirical values and experience. With regard to the position and the coupling of the transducers to the bearing substrate, there is also potential for optimization in future studies. The sensor positioning and its influence on the measurement's sensitivity as well as the influence of the bearing material and design (conventional bearing sleeves and laser cladded bearings) will be subject to future research.

Acknowledgements The authors would like to thank the Ministry of Economic Affairs and Climate Action of Germany, for the financial support granted. They also thank their project partners for the equipment, insight as well as expertise they have provided, which contributed to this joint project.

Supported by:

Federal Ministry
for Economic Affairs
and Climate Action

on the basis of a decision
by the German Bundestag

Funding Open Access funding enabled and organized by Projekt DEAL.

References

1. Umweltbundesamt (2024) Erneuerbare Energien in vol 2023. Daten zur Entwicklung im Jahr, Deutschland
2. Stehly T, Duffy, P (2022) 2021 Cost of Wind Energy Review. National Renewable Energy Laboratory
3. Meyer T (2015) Validation of journal bearings for use in wind turbine gearboxes. inFOCUS: WINDPOWER
4. Thys T, Smet W (2023) Selective assembly of planetary gear stages to improve load sharing. Forsch Ingenieurwes 87(1):275–283
5. van Lier H (2025) Next Generation Plain Bearing Technology for Wind Turbine Gearboxes. In: Conference for Wind Power. Drives, vol 2025. Konferenzband, Aachen
6. Marheineke J (2024) Ermittlung und Bewertung des Verhaltens von hydrodynamischen Gleitlagern bei. Dissertation
7. Boucherit H, Bou-Saïd B, Lahmar M (2017) The effect solid particle lubricant contamination on the dynamic behavior of compliant journal bearings. Lubr Sci 29(7):425–439

8. Tchakoua P, Wamkeue R, Ouhrouche M, Slaoui-Hasnaoui F, Tameghe T, Ekemb G (2014) Wind Turbine Condition Monitoring: State-of-the-Art Review, New Trends, and Future Challenges. Energies 7(4):2595–2630
9. Mokhtari N, Gühmann C (2018) Classification of journal bearing friction states based on acoustic emission signals. Tm – Tech Mess 85(6):434–442
10. Decker T, Jacobs G, Paridon C, Röder J (2024) Condition monitoring for planetary journal bearings in wind turbine gearboxes by means of acoustic measurements and machine learning. Tribol Schmierungstechnik 71:2
11. Baszenski T, Kauth K, Kratz K-H, Gutiérrez Guzmán F, Jacobs G, Gemmeke T (2023) Sensor integrating plain bearings: design of an energy-autonomous, temperature-based condition monitoring system. Forsch Ingenieurwes 87(1):441–452
12. Paeßens J, Kratz K-H, Gemmeke T, Kauth K, Baszenski T, Lehmann B, Jacobs G (2024) Design of a fully integrated sensor system of a plain bearing. Forsch Ingenieurwes 88:1
13. Chmelar J, Petr K, Mossoczy P, Dynybyl V (2020) Experimental study of lubrication film monitoring in a roller bearing by utilization of surface acoustic waves. Tribol Int 141:105908
14. Lindner G, Schmitt M, Schubert J, Krempel S, Faustmann H (2010) On-line surveillance of lubricants in bearings by means of surface acoustic waves. IEEE Trans Ultrason Ferroelectr Freq Control 57(1):126–132
15. Decker T, Jacobs G, Arneth P, Röder J, Raddatz M (2024) Approach towards the condition monitoring of journal bearings using surface acoustic wave technology. Bearing World. Journal 8:
16. Decker T, Jacobs G, Raddatz M, Röder J, Betscher J, Arneth P (2025) Detection of particle contamination and lubrication outage in journal bearings in wind turbine gearboxes using surface acoustic wave measurements and machine learning. Forsch Ingenieurwes 89:1
17. Illner B, Bartel D (2016) Übergangsdrehzahl von Radialgleitlagern – Analytische Bestimmung unter Berücksichtigung der Lagerdeformation. Antriebstechnik
18. IEC 61400:2024-07. Design requirements for wind turbine gearboxes
19. Tesini P, Dzwonczyk-Mertzanis J, Reynders R (2023) A new generation of hydrodynamic plain bearings, enabling the next step in gearbox torque density. In: Conference for Wind Power Drives vol 2023. Conference Proceedings, Aachen